

TECHNICAL RESEARCH REPORT

Sampled-Data Modeling, Analysis and Control of Load-Resonant
DC-DC Converters in Variable Frequency Operation

by C.-C. Fang, E.H. Abed

T.R. 98-53



ISR develops, applies and teaches advanced methodologies of design and analysis to solve complex, hierarchical, heterogeneous and dynamic problems of engineering technology and systems for industry and government.

ISR is a permanent institute of the University of Maryland, within the Glenn L. Martin Institute of Technology/A. James Clark School of Engineering. It is a National Science Foundation Engineering Research Center.

Web site <http://www.isr.umd.edu>

Sampled-Data Modeling, Analysis and Control of Load-Resonant DC-DC Converters in Variable Frequency Operation

Chung-Chieh Fang and Eyad H. Abed
Department of Electrical Engineering
and the Institute for Systems Research
University of Maryland
College Park, MD 20742 USA

Manuscript: September 28, 1998

Abstract

Sampled-data modeling, analysis and control of load-resonant DC-DC converters in variable frequency operation are considered. A general block diagram model is given and then used to obtain a nonlinear sampled-data model reflecting cycle-to-cycle dynamics. An alternative model that reflects half-cycle dynamics is also obtained. The half-cycle model is more compact than the full cycle dynamic model. Because of this, it is used as the basis for the other derivations in the paper. These include: a linearized half-cycle dynamic model, open-loop stability conditions, control-to-output transfer function, open-loop audio-susceptibility, open-loop output impedance, and discrete-time integral controllers achieving line regulation and load regulation.

1 Introduction

Sampled-data modeling, analysis and control of load-resonant DC-DC converters in variable frequency operation are considered. The paper extends to load-resonant converters the work on PWM DC-DC converters reported by the authors in the recent papers [1, 2, 3]. Sampled-data modeling is a powerful tool since it allows representation of detailed dynamics within switching cycles as well as over longer periods of time. The main contribution of this paper is a clear statement of a generally applicable sampled-data model for load-resonant converters, and a formulation of this model in a particularly compact form. The model captures the behavior of various types of load-resonant converters, including the three main classes: the series resonant converter (SRC), the parallel resonant

converter (PRC) and the series-parallel resonant converter (SPRC, also called LCC-type PRC). The paper also includes the derivation of linearized models, stability conditions, discrete-time control designs, and other results all based on the compact sampled-data model.

Previous work on modeling of load-resonant converters has addressed the SRC, PRC and SPRC separately [4, 5, 6, 7, 8, 9, 10, 11]. In the sampled-data approach taken in the present paper, use of vector-matrix notation along with exploitation of inherent symmetry in load-resonant converters leads to a unifying and concise model.

The approach developed here builds on the work of Elbuluk, Verghese and Kassakian [12], who also studied sampled-data modeling and control of load-resonant DC-DC converters. In the present paper, the dynamic models are stated explicitly in a detailed analytical form, as is the symmetry property of load-resonant converters. These features make the models given here straightforward to apply. Moreover, the issues of controller design for line regulation and for load regulation, not considered in [12], are addressed successfully here. (The authors of [12] considered control design for fixed source and load, while in line and load regulation the controller must regulate the output voltage in the presence of uncertainty in source and load.)

The output voltage in a load-resonant converter can be controlled through switching frequency or through phase-shift modulation [13, 14, 15, 16]. This paper addresses only circuits controlled through the switching frequency, which of course results in variable frequency operation. The approach of the paper can also be applied to phase-shift modulated load-resonant converters, which operate at a fixed switching frequency.

The remainder of the paper proceeds as follows. In Sec. 2, a block diagram model is given for the power stage of the load resonant converter in variable frequency operation. In Sec. 3, the block diagram model is used to obtain a nonlinear sampled-data model. In Sec. 4, a half-cycle sampled-data model, more compact than the model of Sec. 3, is derived. The half-cycle model is linearized in Sec. 5. In Sec. 6, the linearized model is used to study open-loop stability. In Sec. 7, the control-to-output transfer function, the open-loop audio-susceptibility, and the open-loop output impedance are derived. In Sec. 8, discrete-time integral control for line and load regulation is

designed. Conclusions are given in Sec. 9.

2 Block Diagram Model

A general block diagram model of the power stage of a load-resonant converter (whether SRC, PRC or SPRC) in variable frequency operation is shown in Fig. 1. In the figure, $A_i \in \mathbf{R}^{N \times N}$, $B_i \in \mathbf{R}^{N \times 1}$, $C, E \in \mathbf{R}^{1 \times N}$, are constant matrices, v_s and v_o are the source and output voltages respectively, and N is the state dimension, which is typically the number of energy storage elements in the converter.

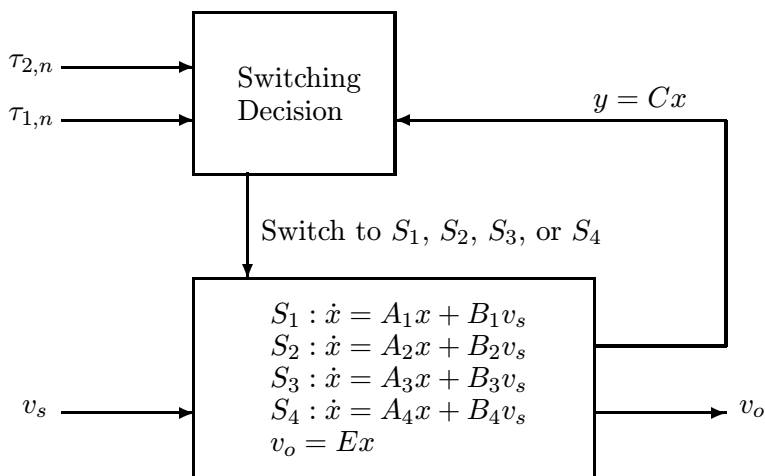


Figure 1: A general power stage model for load-resonant converters

There are generally four stages (S_1 to S_4) per cycle in this class of converter. Consider the operation of the load-resonant converter of Fig. 1 within the n -th cycle. There are two control signals in Fig. 1, $\tau_{1,n}$ and $\tau_{2,n}$: $\tau_{1,n}$ is the combined duration of the first two stages (S_1 and S_2); $\tau_{2,n}$ is the combined duration of the next two stages (S_3 and S_4). Thus the duration of the n -th cycle is $\tau_{1,n} + \tau_{2,n}$. Switching from stage S_1 to stage S_2 , and also switching from stage S_3 to stage S_4 , are controlled through feedback of a single (scalar) circuit variable y . Denote by t_n the beginning instant of the n -th cycle, i.e., let $t_n = \sum_{i=0}^{n-1} (\tau_{1,i} + \tau_{2,i})$. Note that t_n is also the switching instant from S_4 back to S_1 , i.e., from the end of the $(n-1)$ -st cycle to the beginning of the n -th cycle. Switching from stage S_2 to S_3 occurs at time $t_n + \tau_{1,n}$. Note that this switching instant is an *explicit*

function of the control signal $\tau_{1,n}$. However, the switching instants from S_1 to S_2 and from S_3 to S_4 are not explicit, but are determined *implicitly* by the condition $y(t) = 0$. Denote by $d_{1,n}$ and $d_{2,n}$ the duration of stage S_1 and S_3 , respectively. The dynamics within the four stages of the n -th cycle are given as follows:

$$S_1 : \dot{x} = A_1x + B_1v_s \quad \text{for } t \in [t_n, t_n + d_{1,n}) \quad (1)$$

$$S_2 : \dot{x} = A_2x + B_2v_s \quad \text{for } t \in [t_n + d_{1,n}, t_n + \tau_{1,n}) \quad (2)$$

$$S_3 : \dot{x} = A_3x + B_3v_s \quad \text{for } t \in [t_n + \tau_{1,n}, t_n + \tau_{1,n} + d_{2,n}) \quad (3)$$

$$S_4 : \dot{x} = A_4x + B_4v_s \quad \text{for } t \in [t_n + \tau_{1,n} + d_{2,n}, t_{n+1}) \quad (4)$$

along with

$$y(t_n + d_{1,n}) = 0 \quad (5)$$

$$y(t_n + \tau_{1,n} + d_{2,n}) = 0 \quad (6)$$

The above completes the description of the basic block diagram model. However, for the three main types of load-resonant converters (SRC, PRC and SPRC), circuit symmetry implies an interesting and useful relationship among the matrices appearing in the block diagram. This relationship is as follows. The matrices A_i and B_i are related by

$$\begin{aligned} A_3 &= WA_1W & B_3 &= WB_1 \\ A_4 &= WA_2W & B_4 &= WB_2 \end{aligned} \quad (7)$$

here $W \in \mathbf{R}^{N \times N}$ is a projection matrix ($WW = I$) and satisfies $CW = \pm C$, $EW = E$.

A stronger relationship also exists for the the three main types of load-resonant converter, which is stated next but is not needed for the general results to follow. The relationship is useful in computations, however, since it facilitates determination of the matrices for stages S_2 to S_4 from those for stage S_1 .

$$\begin{aligned} A_2 &= WA_1W & B_2 &= B_1 \\ A_3 &= WA_1W & B_3 &= WB_1 \\ A_4 &= A_1 & B_4 &= WB_1 \end{aligned} \quad (8)$$

The next lemma records the fact that relationship (8) is stronger than relationship (7).

Lemma 1 Relationship (8) implies relationship (7).

Proof: From (8),

$$A_4 = A_1 = W(WA_1W)W = WA_2W$$

$$B_4 = WB_1 = WB_2$$

□

Example 1 Take the SPRC of Fig. 2. Let the state be $x = (i_{ls}, v_{cs}, v_{cp}, i_L, v_C)'$. The matrices A_1 , B_1 , C , E and W for the SPRC can be verified to be

$$A_1 = \begin{bmatrix} 0 & \frac{-1}{L_s} & \frac{-1}{L_s} & 0 & 0 \\ \frac{1}{C_s} & 0 & 0 & 0 & 0 \\ \frac{1}{C_p} & 0 & 0 & \frac{1}{C_p} & 0 \\ 0 & 0 & \frac{-1}{L} & 0 & \frac{-1}{L} \\ 0 & 0 & 0 & \frac{1}{C} & \frac{-1}{RC} \end{bmatrix} \quad (9)$$

$$B_1 = \begin{bmatrix} \frac{1}{2L_s} \\ 0 \\ 0 \\ 0 \\ 0 \end{bmatrix} \quad (10)$$

$$C = \begin{bmatrix} 0 & 0 & 1 & 0 & 0 \end{bmatrix} \quad (11)$$

$$E = \begin{bmatrix} 0 & 0 & 0 & 0 & 1 \end{bmatrix} \quad (12)$$

$$W = \begin{bmatrix} -I_{3 \times 3} & 0_{3 \times 2} \\ 0_{2 \times 3} & I_{2 \times 2} \end{bmatrix} \quad (13)$$

The remaining matrices A_2 , B_2 , A_3 , etc., are now easily obtained from Eq. (8).

3 Sampled-Data Dynamics

The following two lemmas are useful in deriving the sampled-data dynamic model. The first lemma gives a relationship between the dynamics in stage S_1 and S_3 , and between the dynamics in stage S_2 and S_4 . Let $\phi_i(\xi, t)$ denote the solution for the state x at time t in the i -th stage starting from

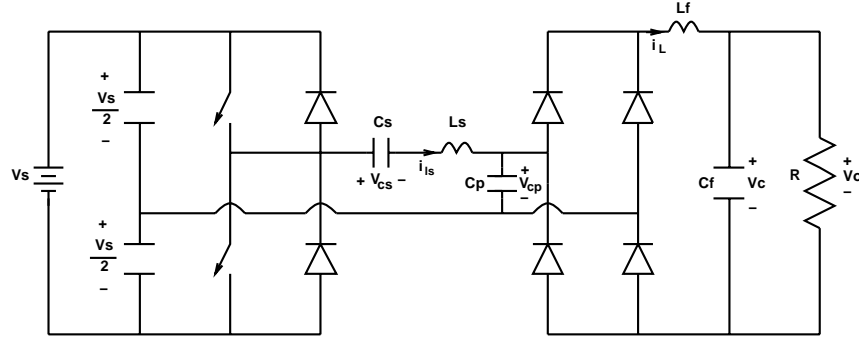


Figure 2: Series-parallel resonant converter with source voltage and resistive load

an initial value ξ with $t = 0$ representing the beginning of the i -th stage. Mathematically, this means

$$\phi_i(\xi, t) = e^{A_i t} \xi + \int_0^t e^{A_i \sigma} d\sigma B_i \quad (14)$$

Lemma 2

$$\phi_1(\xi, t) = W \phi_3(W \xi, t) \quad (15)$$

$$\phi_3(\xi, t) = W \phi_1(W \xi, t) \quad (16)$$

$$\phi_2(\xi, t) = W \phi_4(W \xi, t) \quad (17)$$

$$\phi_4(\xi, t) = W \phi_2(W \xi, t) \quad (18)$$

Proof:

$$\begin{aligned} \phi_1(\xi, t) &= e^{A_1 t} \xi + \int_0^t e^{A_1 \sigma} d\sigma B_1 v_s \\ &= W e^{A_3 t} W \xi + W \int_0^t e^{A_3 \sigma} d\sigma W W B_3 v_s \quad (\text{from (7)}) \\ &= W \phi_3(W \xi, t) \end{aligned}$$

The other claims follow similarly. □

The second lemma asserts that stage S_3 started at ξ will have the same duration as stage S_1 started at $W \xi$.

Lemma 3 *If $C\phi_3(\xi, d) = 0$, then $C\phi_1(W\xi, d) = 0$.*

Proof: If $C\phi_3(\xi, d) = 0$, then

$$\begin{aligned} C\phi_1(W\xi, d) &= CW\phi_3(\xi, d) && \text{(from Lemma 2)} \\ &= \pm C\phi_3(\xi, d) && \text{(from (7))} \\ &= 0 \end{aligned}$$

□

Now consider the operation of the load-resonant converter of Fig. 1 within the n -th cycle. Generally the switching frequency is sufficiently high that the variations in v_s within a cycle can be neglected. Thus, take v_s to be constant within the cycle, and denote its value by $v_{s,n}$. Let $x_n = x(t_n)$, $x_{n+\frac{1}{2}} = x(t_n + \tau_{1,n})$, and $v_{o,n} = v_o(t_n)$.

From Eqs. (1)-(6), Lemma 2 and Lemma 3, the load-resonant converter of Fig. 1 has the following sampled-data dynamic model

$$\begin{aligned} x_{n+\frac{1}{2}} &= f(x_n, v_{s,n}, d_{1,n}, \tau_{1,n}) \\ &= e^{A_2(\tau_{1,n}-d_{1,n})} \left(e^{A_1 d_{1,n}} x_n + \int_0^{d_{1,n}} e^{A_1(d_{1,n}-\sigma)} d\sigma B_1 v_{s,n} \right) \\ &\quad + \int_{d_{1,n}}^{\tau_{1,n}} e^{A_2(\tau_{1,n}-\sigma)} d\sigma B_2 v_{s,n} \end{aligned} \tag{19}$$

$$x_{n+1} = Wf(Wx_{n+\frac{1}{2}}, v_{s,n}, d_{2,n}, \tau_{2,n}) \tag{20}$$

$$\begin{aligned} g(x_n, v_{s,n}, d_{1,n}) &= C \left(e^{A_1 d_{1,n}} x_n + \int_0^{d_{1,n}} e^{A_1(d_{1,n}-\sigma)} d\sigma B_1 v_{s,n} \right) \\ &= 0 \end{aligned} \tag{21}$$

$$g(Wx_{n+\frac{1}{2}}, v_{s,n}, d_{2,n}) = 0 \tag{22}$$

$$v_{o,n} = Ex_n \tag{23}$$

To distinguish this model from the “half-cycle” model given in the next section, the model above will be referred to as the *full-cycle dynamic model*.

4 Half-Cycle Sampled-Data Dynamics

In this section, a half-cycle dynamic model is derived. The main advantage of this model over the full-cycle model (19)-(23) is its compactness. It is also more accurate in that it places less stringent assumptions on the source voltage (v_s assumed constant over *half* of the switching period).

4.1 Nonlinear Model

The authors of [17] used symmetry to simplify their sampled-data model. In the foregoing section, the symmetry property has been stated in the explicit form (7) (or, alternatively, in the stronger form (8)). Motivated by [17], the sampled-data dynamic model (19)-(23) is now simplified using (7).

In Eqs. (19)-(23), the state x_n is mapped to x_{n+1} through an intermediate mapping to $x_{n+\frac{1}{2}}$. Examining the equations, it can be seen that this involves a mapping first by f (in Eq. (19)), then by W (in Eq. (20)), followed again by mappings by f (in Eq. (20)) and W (in Eq. (20)). The repetition of the pattern of f followed by W facilitates rewriting of the model in a more compact form.

Let

$$\begin{aligned} w_{2k-1} &:= x_k \\ w_{2k} &:= Wx_{k+\frac{1}{2}} \end{aligned} \tag{24}$$

Also let $\tau_{2k-1} := \tau_{1,k}$, $\tau_{2k} := \tau_{2,k}$, $d_{2k-1} := d_{1,k}$, $d_{2k} := d_{2,k}$, and $v_{o,k} := v_o(\sum_{i=0}^{k-1} \tau_i)$. Take v_s to be constant within the half-cycle, with value denoted by $v_{s,k}$. With this notation, the sampled-data dynamic model (19)-(23) can be simplified as

$$\begin{aligned} w_{k+1} &= Wf(w_k, v_{s,k}, d_k, \tau_k) \\ g(w_k, v_{s,k}, d_k) &= 0 \\ v_{o,k} &= Ew_k \end{aligned} \tag{25}$$

This simplified model is called the *half-cycle dynamic model* to distinguish it from the full-cycle dynamic model (19)-(23).

4.2 Linearized Model

To obtain a linearized dynamic model from the half-cycle model (25), the fixed point corresponding to the nominal operating condition of the converter must first be found. Given the nominal source voltage V_s and the nominal half switching period τ , the fixed point $(w_k, v_{s,k}, d_k, \tau_k) = (w^0, V_s, d, \tau)$ satisfies

$$w^0 = Wf(w^0, V_s, d, T) \quad (26)$$

$$g(w^0, V_s, d) = 0 \quad (27)$$

This set of nonlinear equations can be solved by Newton's method. Once the fixed point is obtained, the nominal periodic solution $x^0(t)$ of Fig. 1 can be obtained from Eq. (24) along with Eqs. (1)-(4).

Linearizing (25) at the fixed point (w^0, V_s, d, τ) now gives

$$\begin{aligned} \hat{w}_{k+1} &= W(\Phi_o \hat{w}_k + \Gamma_s \hat{v}_{s,k} + \Gamma_\tau \hat{\tau}_k) \\ \hat{v}_{o,k} &= E \hat{w}_k \end{aligned} \quad (28)$$

where

$$\begin{aligned} \Phi_o &= \left. \frac{\partial f}{\partial w_k} - \frac{\partial f}{\partial d_k} \left(\frac{\partial g}{\partial d_k} \right)^{-1} \frac{\partial g}{\partial w_k} \right|_\diamond \\ &= e^{A_2(\tau-d)} \left(I - \frac{((A_1 - A_2)x^0(d) + (B_1 - B_2)V_s)C}{C(A_1 x^0(d) + B_1 V_s)} \right) e^{A_1 d} \\ &= e^{A_2(\tau-d)} \left(I - \frac{(\dot{x}^0(d^-) - \dot{x}^0(d^+))C}{C \dot{x}^0(d^-)} \right) e^{A_1 d} \end{aligned} \quad (29)$$

$$\begin{aligned} \Gamma_s &= \left. \frac{\partial f}{\partial v_{s,k}} - \frac{\partial f}{\partial d_k} \left(\frac{\partial g}{\partial d_k} \right)^{-1} \frac{\partial g}{\partial v_{s,k}} \right|_\diamond \\ &= e^{A_2(\tau-d)} \left(I - \frac{(\dot{x}^0(d^-) - \dot{x}^0(d^+))C}{C \dot{x}^0(d^-)} \right) \int_0^d e^{A_1 \sigma} d\sigma B_1 + \int_0^{\tau-d} e^{A_2 \sigma} d\sigma B_2 \end{aligned} \quad (30)$$

$$\begin{aligned} \Gamma_\tau &= \left. \frac{\partial f}{\partial \tau_k} \right|_\diamond \\ &= A_2 x^0(\tau) + B_2 V_s \\ &= \dot{x}^0(\tau^-) \end{aligned} \quad (31)$$

and where \diamond indicates evaluation at the fixed point.

5 Open-Loop Stability

The next result follows immediately from the half-cycle linearized dynamic model (28).

Theorem 1 *The nominal periodic solution $x^0(t)$ of the load-resonant converter in Fig. 1 is open-loop asymptotically orbitally stable [18] if all of the eigenvalues of $W\Phi_o$ are inside the unit circle of the complex plane.*

A necessary condition for the load-resonant converter to be open-loop asymptotically orbitally stable is given next.

Theorem 2 *Suppose the nominal periodic solution $x^0(t)$ is open-loop asymptotically orbitally stable. Then the following inequality holds:*

$$\left| \frac{C\dot{x}^0(d^+)}{C\dot{x}^0(d^-)} \right| \leq e^{\text{tr}[A_2 - A_1]d - \text{tr}[A_2]\tau} \quad (32)$$

Proof:

$$\begin{aligned} |\det[W\Phi_o]| &= \left| \det[e^{A_1 d} e^{A_2(\tau-d)}] \det\left[I - \frac{(\dot{x}^0(d^-) - \dot{x}^0(d^+))C}{C\dot{x}^0(d^-)}\right] \right| \\ &= e^{-\text{tr}[A_2 - A_1]d + \text{tr}[A_2]\tau} \left| \frac{C\dot{x}^0(d^+)}{C\dot{x}^0(d^-)} \right| \\ &\leq 1 \end{aligned}$$

The claim follows from the last inequality in the sequence above. \square

6 Control-to-Output Transfer Function, Open-Loop Audio-Susceptibility and Output Impedance

From Eq. (28), the control to output (τ to v_o) transfer function is

$$T_{oc}(z) = \frac{\hat{v}_o(z)}{\hat{\tau}(z)} = E(zI - W\Phi_o)^{-1}W\Gamma_\tau \quad (33)$$

Equivalently, with the switching frequency ($f_s = 1/2\tau$) is viewed as the control variable in place of τ , the control-to-output transfer function becomes

$$T_{oc,f}(z) = \frac{\hat{v}_o(z)}{\hat{\tau}(z)} \frac{\hat{\tau}(z)}{\hat{f}_s(z)} = -T_{oc}(z) \frac{1}{2f_s^2} \quad (34)$$

where f_s is the nominal switching frequency.

From Eq. (28), the open-loop audio-susceptibility is

$$T_{os}(z) = \frac{\hat{v}_o(z)}{\hat{v}_s(z)} = E(zI - W\Phi_o)^{-1}W\Gamma_s \quad (35)$$

To calculate the open-loop output impedance, add a fictitious current source i_o (as a perturbation) in parallel with the load. Then the dynamical equations describing the dynamics within S_1 and S_2 are replaced by

$$S_1 : \dot{x} = A_1x + B_1v_s + B_{i1}i_o \quad (36)$$

$$S_2 : \dot{x} = A_2x + B_2v_s + B_{i2}i_o \quad (37)$$

The open-loop output impedance is

$$T_{oo}(z) = \frac{\hat{v}_o(z)}{\hat{i}_o(z)} = E(zI - W\Phi_o)^{-1}W\Gamma_i \quad (38)$$

where

$$\Gamma_i = e^{A_2(\tau-d)} \left(I - \frac{(\dot{x}^0(d^-) - \dot{x}^0(d^+))C}{C\dot{x}^0(d^-)} \right) \int_0^d e^{A_1\sigma} d\sigma B_{i1} + \int_0^{\tau-d} e^{A_2\sigma} d\sigma B_{i2} \quad (39)$$

Given a transfer function in the z domain, say $T(z)$, its effective frequency response [19, p. 93] is

$$T_{\text{effective}}(j\omega) = T(e^{j\omega\tau}) \quad (40)$$

valid in the frequency range $|\omega| < \frac{\pi}{\tau}$.

Example 2 (*Control-to-output frequency response of SPRC*, [20]) Consider again the SPRC power stage of Example 1, shown in Fig. 2, with $V_s = 100V$, $L_s = 5.2\mu H$, $C_s = C_p = 5.5nF$, $L_f = 13\mu H$,

$C_f = 1\mu F$, $R = 26.507\Omega$, the nominal switching frequency $f_s = 1.6713MHz$, and $\tau = 1/2f_s = 2.9917 \times 10^{-7}sec$.

Take the switching frequency as the control variable. From Eqs. (34) and (40), and performing a normalization as in [20]), the normalized control-to-output frequency response is

$$\frac{1}{2\pi\sqrt{L_s C_s}} T_{oc,f}(e^{j\omega\tau}) = -E(e^{j\omega\tau}I - W\Phi_o)^{-1}W\Gamma_\tau \left(\frac{1}{2f_s^2}\right) \left(\frac{1}{2\pi\sqrt{L_s C_s}}\right) \quad (41)$$

where $1/(2\pi\sqrt{L_s C_s})$ is a normalizing factor.

In obtaining the control-to-output frequency response above, the sampled-data model was used directly along with the formula (40). This approach is called the S method in [21, 2]. In an alternative approach [21, 2], the sampled-data model can first be “lifted” to a continuous-time linear model that is consistent under sampling with the sampled-data model. The transfer function of interest is then evaluated for the obtained continuous-time model. If the pair $(W\Phi_o, -W\Gamma_\tau/(4\pi\sqrt{L_s C_s}f_s^2))$ is transformed (“lifted”) to a continuous-time pair (Φ^c, Γ^c) , then the control-to-output frequency response is

$$E(j\omega I - \Phi^c)^{-1}\Gamma^c \quad (42)$$

This approach is called the SC method in [21, 2].

Figures 3 and 4 show the control-to-output frequency response obtained using the S and SC methods, both of which agree well with the results in [20]. The agreement of the S or SC methods is due to the high switching frequency.

7 Discrete-Time Integral Control of Load-Resonant Converters

In this section, a discrete-time integral controller is proposed for achieving line and load regulation. Most feedback loops in DC-DC converters contain an integrator (continuous-time) to ensure line and load regulation [22]. Here a discrete-time integral controller is proposed:

$$\begin{aligned} v_{k+1} &= v_k + V_{SET} - Ew_{k+1} \\ \tau_k &= -K_1 w_k - K_2 v_k \end{aligned} \quad (43)$$

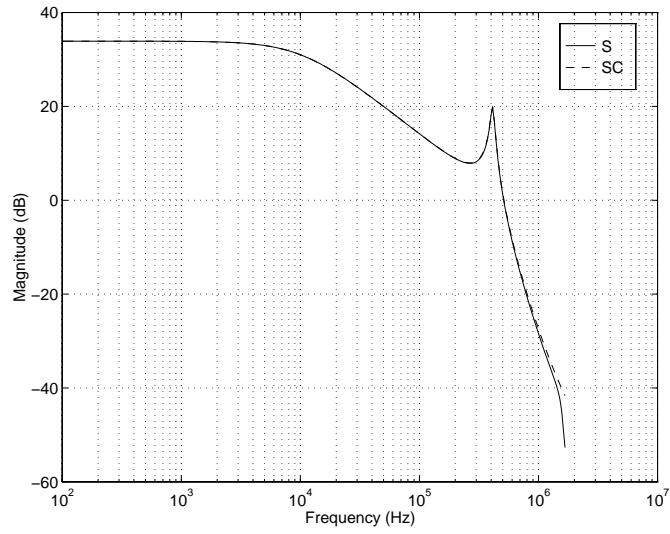


Figure 3: Control-to-output magnitude response obtained using the S and SC methods

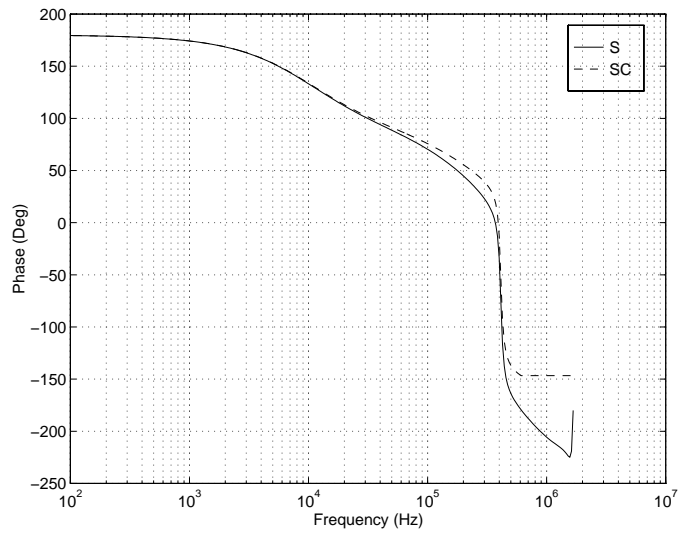


Figure 4: Control-to-output phase response obtained by the S and SC methods

where v_k is the state of integral controller, and V_{SET} is the set-point output voltage. If the closed-loop system (25), (43) is stabilized, then $v_o = Ew = V_{\text{SET}}$ in steady state. Thus output voltage regulation is achieved.

Since different switching periods will cause the circuit to operate in different modes, a limiter on τ_n needs to be imposed, which is not shown explicitly in Eq. (43). For example in the above-resonance mode, an upper limit on τ_n must be imposed.

The closed-loop system (25), (43) has the following linearized dynamic model at the fixed point $(w_k, v_{s,k}, d_k, \tau_k) = (w^0, V_s, d, \tau)$:

$$\begin{aligned} \begin{bmatrix} \hat{w}_{k+1} \\ \hat{v}_{k+1} \\ \hat{v}_{o,k} \end{bmatrix} &= \begin{bmatrix} W\Phi_o & 0 \\ -E & 1 \end{bmatrix} \begin{bmatrix} \hat{w}_k \\ \hat{v}_k \end{bmatrix} + \begin{bmatrix} W\Gamma_\tau \\ 0 \end{bmatrix} \hat{\tau}_k + \begin{bmatrix} W\Gamma_s \\ 0 \end{bmatrix} \hat{v}_{s,k} \\ &= E\hat{w}_k \end{aligned} \quad (44)$$

To stabilize the system, the pair $(\begin{bmatrix} W\Phi_o & 0 \\ -E & 1 \end{bmatrix}, \begin{bmatrix} W\Gamma_\tau \\ 0 \end{bmatrix})$ should be stabilizable. This is equivalent to the pair $(W\Phi_o, W\Gamma_\tau)$ being stabilizable and the matrix $\begin{bmatrix} W\Phi_o - I & W\Gamma_\tau \\ E & 0 \end{bmatrix}$ being of full rank [23].

From Eq. (44), the audio-susceptibility of the closed-loop system (25), (43) is

$$T_{os}(z) = \begin{bmatrix} E & 0 \end{bmatrix} (zI - (\begin{bmatrix} W\Phi_o & 0 \\ -E & 1 \end{bmatrix} - \begin{bmatrix} W\Gamma_\tau \\ 0 \end{bmatrix} \begin{bmatrix} K_1 & K_2 \end{bmatrix}))^{-1} \begin{bmatrix} W\Gamma_s \\ 0 \end{bmatrix}$$

Similarly, the output impedance of the closed-loop system (25), (43) is

$$T_{oo}(z) = \begin{bmatrix} E & 0 \end{bmatrix} (zI - (\begin{bmatrix} W\Phi_o & 0 \\ -E & 1 \end{bmatrix} - \begin{bmatrix} W\Gamma_\tau \\ 0 \end{bmatrix} \begin{bmatrix} K_1 & K_2 \end{bmatrix}))^{-1} \begin{bmatrix} W\Gamma_i \\ 0 \end{bmatrix}$$

Example 3 (*Integral control of an SPRC*) In this example, line and load regulation of the SPRC in Example 2 is considered. The goal of the control design here is to regulate the output voltage at 24V, under 20% variation from the nominal values of the source voltage and load.

From Eqs. (28) and (29), the circuit has open-loop poles at -0.6949 , $0.6915 \pm 0.68i$, 0.5731 and

0.9808. Because of the complex poles close to the unit circle, the open-loop dynamics is expected to be slow.

Figures 5 and 6 show the output voltage response without control as the source voltage and the load respectively are step-changed. The response is slow, and the line and load regulation are not good.

Next, integral control is applied to the system. To prevent the control signal from being too large, the closed loop poles are assigned at 0, 0, 0, 0, 0.5, and 0.5.

Figures 7 and 8 show the output voltage response under integral control as the source voltage and the load, respectively, are step-changed. The response is fast and the output voltage is regulated at 24V.

Figures 9 and 10 show the audio-susceptibility and output impedance, respectively, with and without control. A significant improvement is achieved with integral control.

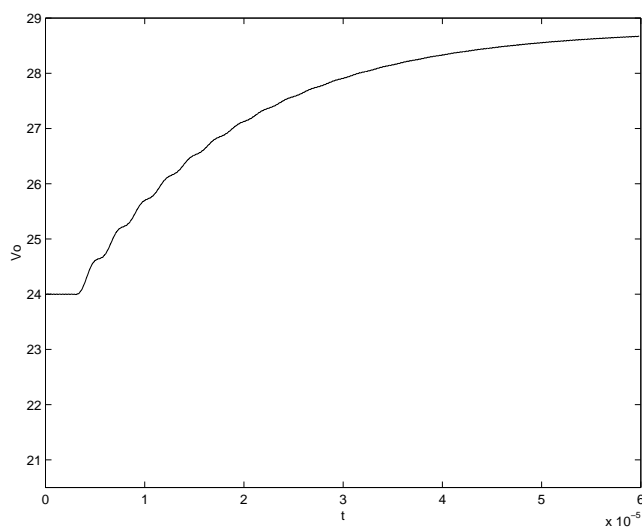


Figure 5: Output voltage response without control when the source voltage changes from 100V to 120V at $t = 2.7 \times 10^{-6} s$

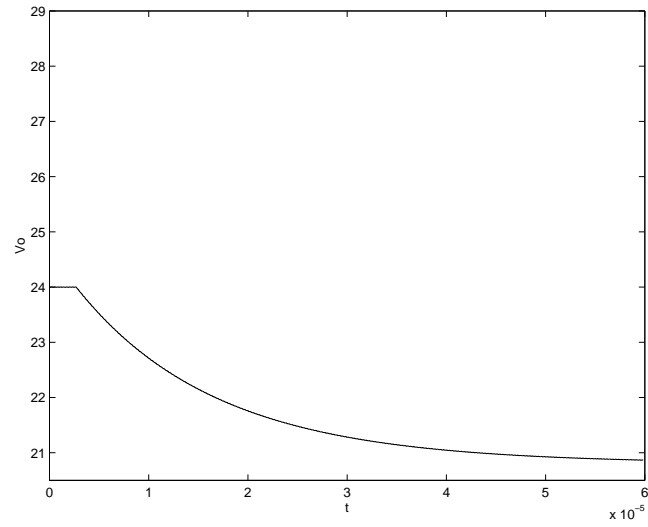


Figure 6: Output voltage response without control when the load changes from 26.5Ω to 21.2Ω at $t = 2.7 \times 10^{-6}s$

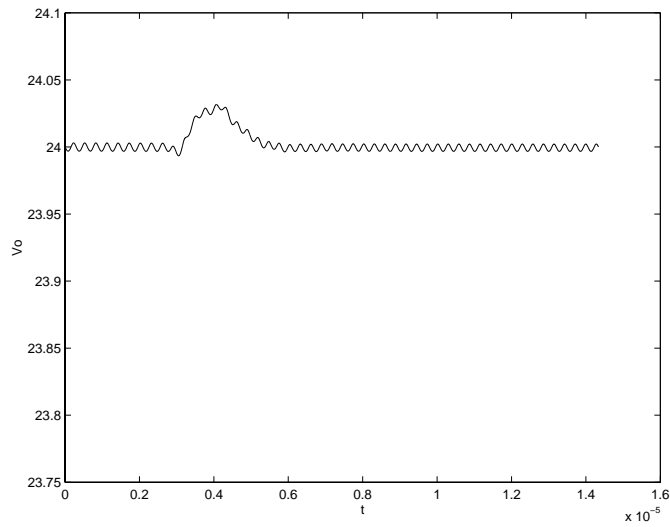


Figure 7: Output voltage response with control when the source voltage changes from $100V$ to $120V$ at $t = 2.7 \times 10^{-6}s$

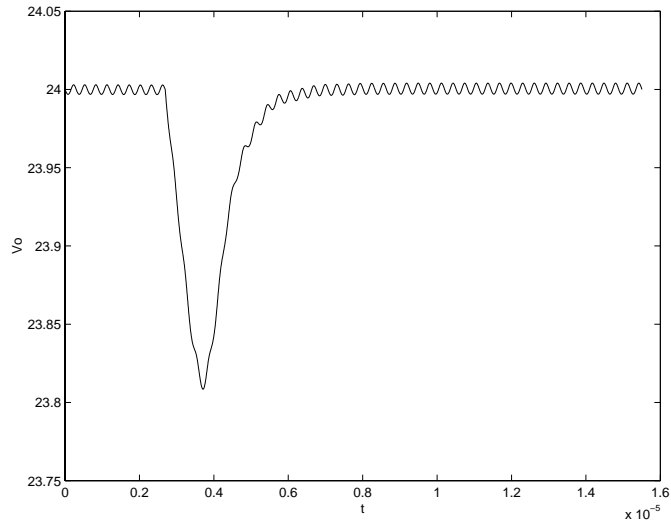


Figure 8: Output voltage response with control when the load changes from 26.5Ω to 21.2Ω at $t = 2.7 \times 10^{-6}s$

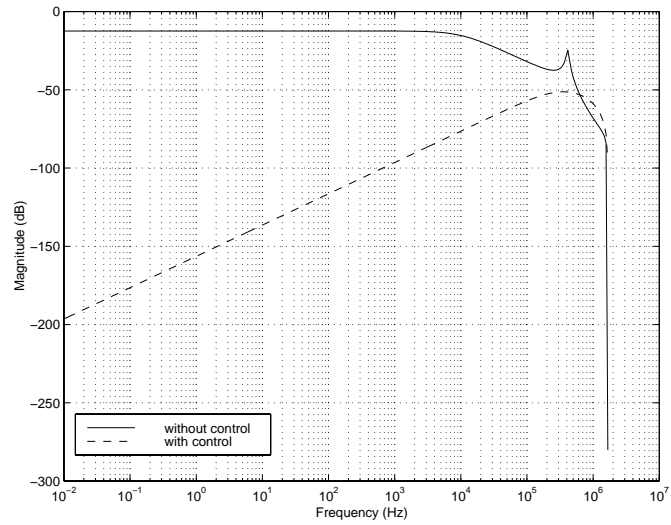


Figure 9: Audio-susceptibility of uncontrolled and controlled SPRC

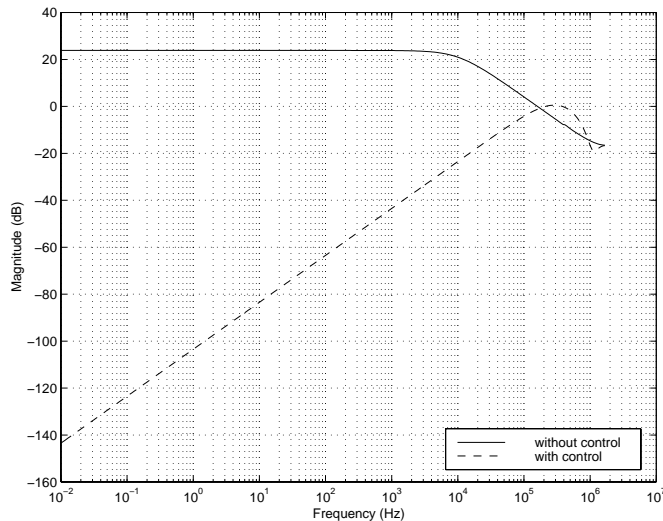


Figure 10: Output impedance of uncontrolled and controlled SPRC

8 Concluding Remarks

The load-resonant DC-DC converter in variable frequency operation has been modeled, analyzed and controlled using the sampled-data approach. The paper extends to load-resonant converters recent work of the authors on sampled-data modeling and analysis of PWM converters. Nonlinear, linearized and simplified half-cycle sampled-data models were given. These models are expressed in concise vector-matrix form. The sampled-data approach employed is systematic and applies to different types of load-resonant converters. By using discrete-time integral control, line and load regulation of the converter has been achieved.

Acknowledgments

This research has been supported in part by the the Office of Naval Research under Multidisciplinary University Research Initiative (MURI) Grant N00014-96-1-1123, the U.S. Air Force Office of Scientific Research under Grant F49620-96-1-0161, and by a Senior Fulbright Scholar Award.

References

- [1] C.-C. Fang and E.H. Abed, "Sampled-data modeling and analysis of PWM DC-DC converters I. Closed-loop circuits," preprint, Feb. 1998.
- [2] C.-C. Fang and E.H. Abed, "Sampled-data modeling and analysis of PWM DC-DC converters II. The power stage," preprint, Feb. 1998.

- [3] C.-C. Fang and E.H. Abed, "Sampled-data modeling and analysis of PWM DC-DC converters under hysteretic control," preprint, March 1998.
- [4] V. Vorperian and S. Čuk, "Small signal analysis of resonant converters," in *IEEE Power Electronics Specialists Conf. Rec.*, 1983, pp. 269–282.
- [5] R.J. King and T.A. Stuart, "Small-signal model for the series resonant converter," *IEEE Transactions on Aerospace and Electronic Systems*, vol. AES-21, no. 3, pp. 301–319, 1985.
- [6] M.G. Kim and M.J. Youn, "A discrete time domain modeling and analysis of controlled parallel resonant converter," *IEEE Transactions on Industrial Electronics*, vol. 38, no. 1, pp. 32–40, 1991.
- [7] K. Siri, *Small Signal Analysis of Resonant Converters and Control Approaches for Parallel Connected Converter Systems*, Ph.D. thesis, University of Illinois at Chicago, 1991.
- [8] E.X. Yang, F.C. Lee, and M. M. Jovanovic, "Small-signal modeling of LCC resonant converter," in *IEEE Power Electronics Specialists Conf. Rec.*, 1992, pp. 941–950.
- [9] V. Agarwal and A.K.S. Bhat, "Large signal analysis of the LCC-type parallel resonant converter using discrete time domain modeling," *IEEE Transactions on Power Electronics*, vol. 10, no. 2, pp. 222–238, 1995.
- [10] V. Agarwal and A.K.S. Bhat, "Small signal analysis of the LCC-type parallel resonant converter using discrete time domain modeling," *IEEE Transactions on Industrial Electronics*, vol. 42, no. 6, pp. 604–614, 1995.
- [11] I. Batarseh, C. Megalemos, and M. Sznaiier, "Small signal analysis of the LCC-type parallel resonant converter," *IEEE Transactions on Aerospace and Electronic Systems*, vol. 32, no. 2, pp. 702–713, 1996.
- [12] M.E. Elbuluk, G.C. Verghese, and J.G. Kassakian, "Sampled-data modeling and digital control of resonant converters," *IEEE Transactions on Power Electronics*, vol. 3, no. 3, pp. 344–354, 1988.
- [13] I.J. Pitel, "Phase-modulated, resonant power conversion techniques for high-frequency link inverters," *IEEE Transactions on Industry Applications*, vol. IA-22, no. 6, pp. 1044–1051, 1986.
- [14] F.-S. Tsai and F.C. Lee, "Constant-frequency phase-controlled resonant power processor," in *Conference Record of the 1986 IEEE Industry Applications Society Annual Meeting*, 1986, pp. 617–622.
- [15] A.K.S. Bhat, "Fixed frequency PWM series-parallel resonant converter," in *Conference Record of the IEEE Industry Applications Society Annual Meeting*, 1989, pp. 1115–1121.
- [16] C.Q. Lee, S. Sooksatra, and R. Liu, "Constant frequency controlled full-bridge LCC-type parallel resonant converter," in *Sixth Annual Applied Power Electronics Conference and Exposition. Conference Proceedings*, 1991, pp. 587–593.
- [17] G.C. Verghese, M. Elbuluk, and J.G. Kassakian, "A general approach to sample-data modeling for power electronic circuits," *IEEE Transactions on Power Electronics*, vol. 1, no. 2, pp. 76–89, 1986.

- [18] H.K. Khalil, *Nonlinear Systems*, Macmillan, New York, 1992.
- [19] A.V. Oppenheim and R.W. Schaffer, *Discrete-Time Signal Processing*, Prentice-Hall, Englewood Cliffs, NJ, 1989.
- [20] A.J. Forsyth, Y.K.E. Ho, and H.M. Ong, “Comparison of small-signal modelling techniques for the series-parallel resonant converter,” in *Proceedings of 5th International Conference on Power Electronics and Variable-Speed Drives*, 1994, pp. 268–273.
- [21] C.-C. Fang, *Sampled-Data Analysis and Control of DC-DC Switching Converters*, Ph.D. thesis, University of Maryland, College Park, 1997.
- [22] R.W. Erickson, *Fundamentals of Power Electronics*, Chapman and Hall, New York, 1997.
- [23] C.-C. Fang and E.H. Abed, “Feedback stabilization of PWM DC-DC converters,” preprint, March 1998.